Storm Surf Phenomena at the Western Coast of Sylt Island

BY FRITZ BÜSCHING

Summary

Based on existing surge data measured in the coastal area of Westerland/Sylt, physical principles of storm surf are investigated using the model of resonant basin oscillations including reflection and anomalous dispersion phenomena. Contrary to respective previous publications, which are dealing with the averaged anomalous dispersion effect (ADE) considering nearly the whole energy containing frequency range, particular attention has been paid on special spots of resonance. The latter are characterized by maximum gradients dc/df > 0, which even better comply with the analogue of resonant absorption of electromagnetic waves.

Two different model conceptions had been found appropriate with respect to (partial) standing waves forming elements of resonant basin oscillations.

In natural field conditions: Incident waves from the sea (stimulator) resonating with partial standing half-waves in a definable water basin (resonator), and

in a scale model: The wave maker (stimulator) resonating with partial standing quarter-waves in the wave tank (resonator).

At high energetic storm surges, besides multimodal energy spectra even a broad unimodal energy-spectrum can be represented by multiple neighboring spots of resonances together with alternating sequences of normal and anomalous dispersion.

The occurrence of partial standing waves of considerable extent is supporting the author´s finding of a „storm wave resonance". Local sand removal rates have been estimated as 1.5m/h at heavy storm surges.

Zusammenfassung

Auf der Grundlage vorhandener Sturmflut-Messdaten aus dem Bereich der Uferlinie vor Westerland werden Gegebenheiten der Sturmbrandung am Modell resonanter Beckenschwingungen hinsichtlich der Ausprägung von Reflexion, Resonanz und anomaler Dispersion untersucht.

Im Unterschied zu diesbezüglichen früheren Publikationen, die den Effekt der anomalen Dispersion (ADE) bezüglich eines vorgegebenen Frequenzbandes als *globales* Phänomen behandelt hatten, ist das Augenmerk auf *ausgezeichnete* Resonanzstellen der spektralen Peaks gerichtet. Letztere sind jeweils durch einen maximalen Gradienten dc/df > 0 gekennzeichnet, womit die Analogie zur *Resonanzabsorption elektromagnetischer Wellen* noch dezidierter erfüllt ist. Hinsichtlich der *Positionierung* partiell stehender Wellen als Elemente resonanter Beckenschwingungen werden dabei zwei unterschiedliche Modellvorstellungen unterschieden.

In der *Natur* : die Resonanz der *von See kommenden Wellen* (Erreger) mit *partiell stehenden Halbwellen* in einem *abgrenzbaren Beckenvolumen* (Resonator) und

im *verkleinerten Modell* : die Resonanz des *Wellenerzeugers* (Erreger) mit *partiell stehenden Viertelwellen im Wellenkanal* (Resonator).

Neben multimodalen Energiedichtespektren können auch (breite) *monomodale* Energiedichtespektren bei resonanten Beckenkonfigurationen *mehrere benachbarte* Resonanzstellen repräsentieren, wobei zugehörige Abschnitte anomaler und normaler Dispersion im *gesamten Frequenzbereich hoher Energiedichten* einander abwechseln.

Das Auftreten partiell stehender Wellen bedeutenden Ausmaßes *unterstützt* die These des Autors von der „Sturmwellenresonanz". Örtliche Abbruchraten von der Randdüne Westerland werden für extreme Sturmflutwasserstände zu 1,5m/h abgeschätzt.

K e y w o r d s

Partial reflection, resonance, storm surge, surf zone, dune, sand removal, co-cumulative spectrum, energy spectrum, anomalous dispersion.

C o n t e n t s

1. I n t r o d u c t i o n

Since coastal research work concentrates on laboratory investigations using prototype scale 1:1 to be carried out in large scale facilities, natural time sequences of wave measurements have been documented relatively seldom. Hence, the lack of knowledge on extreme natural conditions has not been reduced sufficiently since the 1970ties.

Therefore the author once again refers to the inspection of the storm surge event of December 13 and 14, 1973 on Sylt Island / North Sea [1].

Under the topic of "Energy Dissipation Processes Of Surf Zones", then at the first time in Germany, electronic pressure devices and current meters had been placed in the surf zone. Especially the author´s measurements had been stored on magnetic tape with the advantage that the data could be analyzed at a high level of reliability in using *automatic* devices exclusively [2].

In particular the water level elevations had been measured synchronously at two stations 15m apart from each other in a coast perpendicular measuring profile (at distances 100m and 85m from the foreshore dune) to be seen from Fig.01, see also Appendices 4.1 and 4.2.

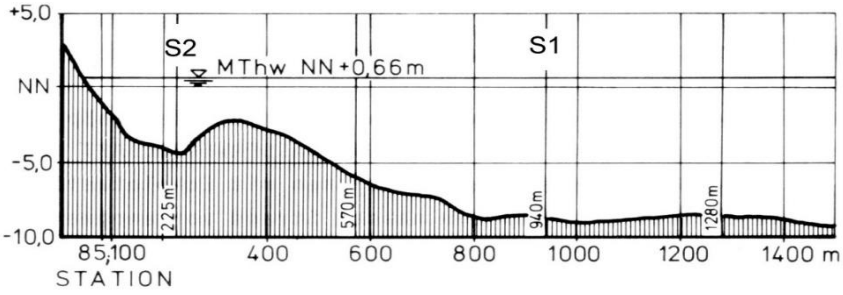

Fig.01: Measuring profile Westerland, North Sea/ Sylt Island, 1973. Surf zone measuring stations 100m and 85m versus foreshore stations S1 and S2.

In the past related data had been published by the author associated with the following topics:

1974	Data Analysis, Water Levels, Orbital Velocities, Normalized Energy Spectra [1], [2];
1975, 1976	Surf Spectra, Co-cumulative energy spectra [3], [4];
1978, 1979	Wave Deformation, Anomalous Dispersion [5], [6], [7];
1980	Anomalous Dispersion due to flow-induced Frequency Shifts [8], [9];
1982, 1983	Resonance Absorption Analogue Electromagnetic Waves [10], [11];
1996	Different Anomalous Dispersion Effects [12], [13];
2003, 2005	Wave Basin Resonances. [14], [15].

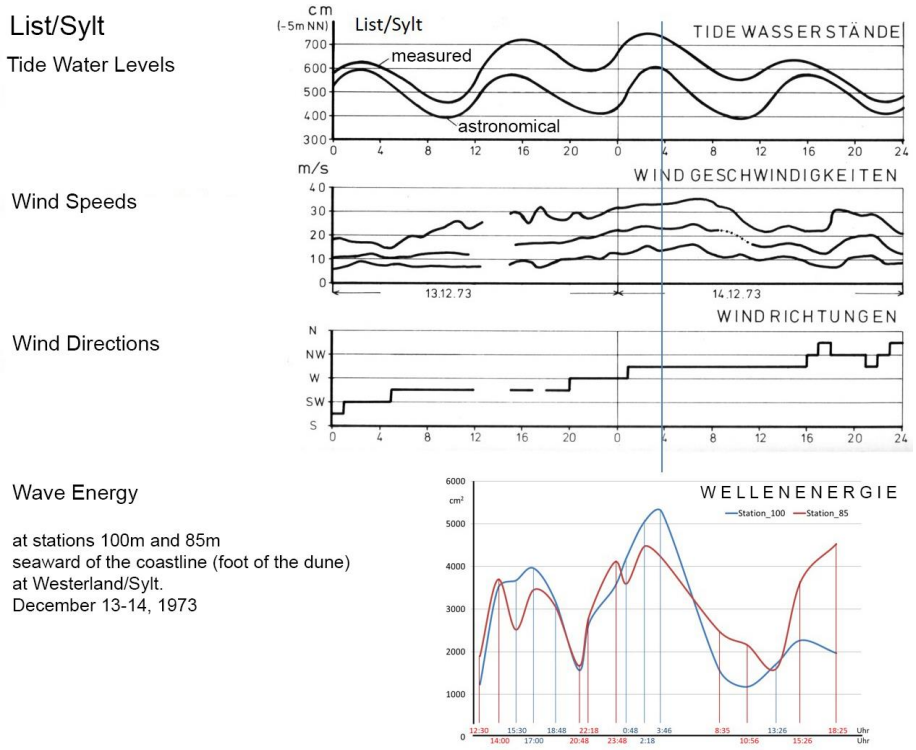

Fig.02: Water levels, wind speeds and wind directions at List/Sylt
and surf wave energies at Westerland/Sylt
during storm surges on December 13-14, 1973.

Measurements at that time had been marked by high energetic surf spectra (cf. Annex 4.3), forming the basis for calculating transfer functions between both tide-gauge records. As a result *phase velocity spectra* [5] had been found, showing the gradient $dc/df > 0$ contradicting the classical dispersion relation.

On this matter error calculations had been performed by Büsching, F. & Speranski, N. S., also considering field investigations by other researchers. As a result the reliability of the anomalous dispersion effect (ADE) could be related to two frequency ranges, separated by the spectral peak frequency f_P.

Especially the ADE at $f > f_P$ was recognized as a second order effect, whereas at $f < f_P$ the ADE is accompanied by partial standing waves, [12] [13]. On account of the fact that the low frequency ADE had shown to be significantly pronounced at heavy storm surge action at Sylt Island, the author had found it necessary to discuss the analogy on *resonance absorption of electromagnetic waves* once again, since such an analogy had been proved with respect to basin oscillations in the wave tank of Bielefeld University of Applied Sciences (BUAS) [14].

The analogue issue normally is recognized in the fact that at both kinds of waves (electromagnetic and water waves) there are frequency ranges at which *resonance, absorption and anomalous dispersion* occur together.

Although such *resonance behavior* combined with an ADE had been found by the author in a wave tank, whose front and rear ends had simply been approximated by *vertical* walls [14], the thesis of resonance could even be *reinforced* by applying boundary conditions closer to the *real inclined* ones at the rear end: the used basin configuration had been found appropriate for rather steep slopes [16], [17], because phase jumps $\Delta\varphi$ (= phase shifts between incident and reflected waves) had been observed at the reflection process from slopes 1:3 and 1:2, see further below.

The significant meaning of the *phase shift* $\Delta\varphi$ occurring together with reflection - depending on frequency, slope angle and surface properties – had been recognized by the author when investigating *hollow revetment structures* [18] [19]. Especially it had come out from such tests of scale 1:5 that by means of appropriate interference of hollow blocks with the washing movement not only the wave run-up and the breaker height could significantly be reduced, but also the breaker type and its relative position on the slope face was modified.

This is why the author had arrived at a more differentiated perspective regarding the breaking process of waves at rather steep sloping structures in such a way that a variable phase difference between the incident and reflected wave plays an important part in the reflection process [16], [18]:

> In the author's view not only the phenomena of reflection and dissipation have to be considered for describing the wave breaking process, but transmission too; just like an analogue of electromagnetic waves at uniform planar interfaces: In the course of the dissipating wave breaking process, a wave pulse of transmission evolves from the initial incident wave at the landward side, while a reflected wave is produced on the seaward side at the same time. The wave pulse of transmission is characterized by a wave height $H_t < H_i$, the wave length $L_t < L_i$ and phase velocity $c_t < c_i$, and also the reflected wave height is $H_r < H_i$.
>
> In this process it is essential that evidently due to the law of conservation of momentum, the positive water level deflection of the transmitted wave pulse postulates locally a negative water level deflection of the reflecting wave. Hence, the superimposition of incident and reflected waves results in a partially standing wave comprising of a *phase jump* $\Delta\varphi$, whose manifestation decides on the one hand on the partial clapotis' position relative to the structure, and on the other hand at least may be decisive for the breaker's kinematics.

The subsequent discussion is motivated by the intention to reassess existing measuring data by considering the new findings illustrated above. Actually the existence of a *Storm Wave Resonance* Effect (SWR) discussed in [14] and [15] is supported.

2. Resonant Basin Oscillations at Natural Coasts

Considering such conditions, the investigations on Storm Wave Resonance (SWR) [14] had been limited to 5 of 16 storm surge measurements, within a time span of 30 hours, at which *maximum water levels* had been measured, cf. Fig.02.

Because of the very powerful spectra, it appeared obvious to assume that mechanisms, known so far only from long-wave excitations of water volumes in bights or harbors (eventually by Tsunami), can be the reason for *higher-frequency* maritime excitations as well.

In this connection it is of particular importance that even harbors with exceedingly irregular shapes do oscillate with remarkable regularity and do not need the boundary conditions of an open or semi-enclosed basin in order to produce distinct regular standing wave patterns. Moreover already Bascom [20] and others report that water masses on the continental shelf can perform seiches-like oscillations also. And it is hardly surprising that the reason for the generation of the largest waves ever recorded by scientific instruments in the 'Rockall Trough' (West of Scotland) is assumed to be due to unknown resonance mechanisms [21].

Not to forget 'edge waves', which are interpreted by researchers as a resonance phenomenon with the particularity that they often appear as *sub-harmonic* coast parallel oscillations [22].

Actually the author was able to show that for the generation of resonant conditions of *various* volumes of water (like the content of a wave flume or the volume contained in the measuring profile of Fig. 01), in a first approximation it is sufficient to have a *prismatic* volume of water (in a basin bounded by *vertical walls*, Fig.03) acting as a resonator.

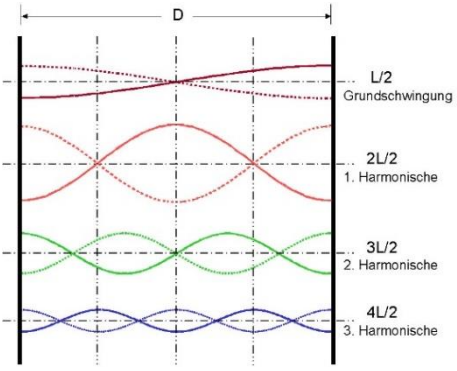

Fig.03: The first 4 theoretical mode shapes of natural oscillations in a basin confined by vertical walls at the front end and at the rear end.

It is known that in this case the natural frequencies, belonging to the mode shapes of Fig.03 (perfect standing waves), can be calculated using Merian's (1828) formula (01)

$$f\left[Hz\right] = \left(n+1\right)\cdot\frac{c}{2\cdot D} \qquad (1)$$

Where
D = horizontal wall distance
c =wave celerity
n = harmonic number

n = 0 denotes the fundamental oscillation and n = 1, 2, 3…are named first, second, third harmonic etc.

Contrary to Merian, who simply used $c = \sqrt{gd}$ in his formula, at a spectral treatment it is necessary to use the quasi measured phase velocities (depending on frequency) c(AD)(f), - especially for the purpose of extracting the harmonic numbers n(f).

Based on model experiments of scale 1:5, the author had claimed that besides Positive Total Reflection (PTR) at water waves there exists also the theoretical limiting case of Negative Total Reflection (NTR) [16]. Hence, the circumstances for its approximate occurrence in nature can be described by defining a *complex reflection coefficient* (CRC) $\Gamma = C_r e^{i\Delta\varphi}$ [18].

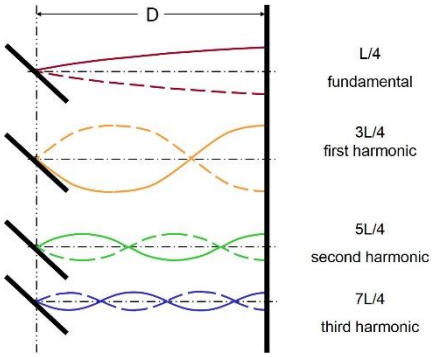

Fig.04: The first 4 theoretical mode shapes of natural oscillations of a basin, confined by a vertical wall at the front end and by a slope at the distance D.

More specifically: The investigations in a wave tank had shown that close to rather steep slopes an *incomplete node* (in accordance with a minimum of energy) exists more distinctly than an *incomplete loop* (in accordance with a maximum of energy). Thus evidently a *phase jump* occurs.

Accordingly the natural frequencies of a wave tank, approximated by a basin confined by a vertical wall (at the hinge of the wave maker) and an inclined wall (slope) (at the opposite end), can be estimated more appropriately in using the following formula, considering the standing wave mode shapes of Fig.04, than by formula (1).

$$f\,[Hz] = (2n+1)\cdot\frac{c}{4\cdot D} \qquad (2)$$

Solving Formula (2) with respect to harmonic numbers n(f)[-], yields formula (3):

$$n(f)[-] = \frac{2\cdot D\cdot f}{c} - 0{,}5 \qquad (3)$$

As an example concerning this matter, the improved results of basin oscillations of the wave tank used are shown in Fig.05 [16].

In that regard, it should be pointed out that resonant higher harmonics (partial standing waves) occurred with ordinal numbers $4 \le n \le 9$, which had been found in using formula (3) applying the horizontal distance D = 11.638m.

Moreover, it is to be seen clearly that the mode numbers correspond to sub-frequency ranges, which are marked by anomalous dispersion dc/df > 0 and thus by resonance.

Close to the point of resonance the measured component-lengths L(AD) (AD = anomalous dispersion)[1] tend to a fairly constant value, which is obviously the reason for the phase velocities c(AD) to behave anomalously.
As a consequence L(AD) and c(AD) progressively differ from the theoretical values L(ND) and c(ND), with *decreasing* frequency *downwards* and with *increasing* frequency *upwards*.

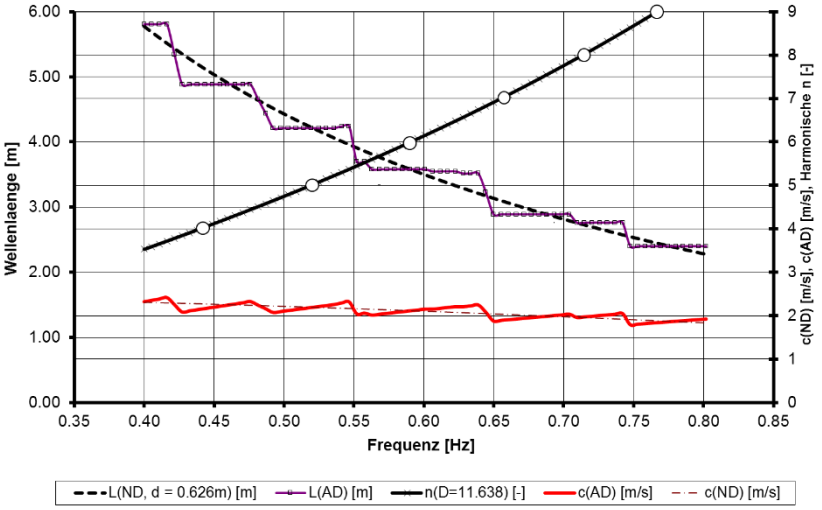

Fig.05: Component length L, phase velocities c and harmonic numbers n plotted with frequency.

It should be noted here that the calculated resonance-frequencies match *fairly exactly* the intersection points of L(ND) and L(AD) on the one hand, and of c(ND) and c(AD) on the other - *only* for waves of lengths 3.58m (n = 5; f ≈ 0.52Hz) and 4.21m (n = 6; f ≈ 0.59Hz), which carry maximum wave energies. That feature is well known also from resonance absorption of electromagnetic waves in dielectrics [11]. Among other things, the increasing deviation for higher and lower frequencies may be due to the fact that the *spectral analysis* is not sufficiently reliable at the remaining harmonic resonance frequencies in the above mentioned sense.

At this place it has to be mentioned that the reported results on *negative reflection* at a slope 1:3 are due to the boundary conditions existing in the BUAS wave tank including such as non-quantifiable (frequency dependent) damping effects. More details are contained in [14] [15] [16] [17].

According to the definition of a Complex Reflection Coefficient (CRC) $\Gamma = C_r e^{i\Delta\varphi}$ (with magnitude $C_r = H_r/H_i$ and phase(difference) $\Delta\varphi$) the negative reflection condition is assigned

[1] The expression in brackets (AD) had been used in earlier publications and denotes values to be retraced to measurements (quasi measurements = derived from a different measured quantity) basically characterizing anomalous dispersion (dc/df > 0 and dc/dL < 0 respectively). Contrary the parenthesized expression (ND) stands for normal dispersion (dc/df ≤ 0 and dc/dL ≥ 0 respectively) according to the classical dispersion relation.

as the condition at which the incomplete node of a partial standing wave is closer to the reflecting slope than the incomplete loop nearest to the slope - thus at phase differences $90^0 < \Delta\varphi < 270^0$.

At storm surge conditions on natural coasts, however, the negative reflection will hardly occur impressively. Either the local boundary conditions support the formation of *surging breakers*.

In the case of reflection from the foot of the dune at a slope angle ≥ 30°or from the bluff, however, in nature almost exclusively positive reflection will occur. As shown in the mentioned investigations, this is not true to the frequency range 0,4Hz ≤ f ≤ 0,8Hz (wave lengths L < 6m). Such a presumption can, however, be extrapolated, for instance, from the results on a smooth revetment 1:3 for natural wave lengths L > 12m [18]

The author summarizes in this respect that the formation of positive or negative reflection in a *natural scale* is *predominantly* governed by frequency (besides other influences).

In other words, with respect to the positive reflection, the effect of surface roughness of a reflecting structure is the less important the longer the waves are.

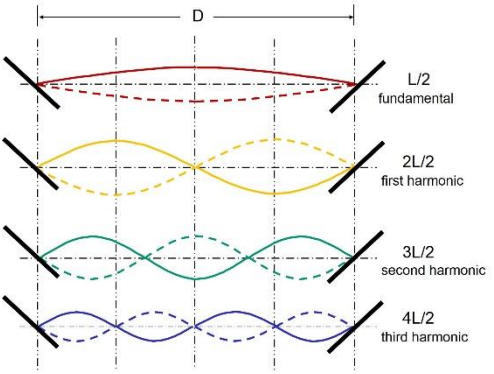

Fig.06: The first 4 *theoretical* mode shapes of natural oscillations of a water body assigned by sloping walls, due to which phase jumps of $\Delta\varphi = 180^0$ and thus negative total reflection occurs.

If the storm wave resonance (SWR) at Sylt Island (cf. [14] and [15]) is mainly regarded to be due to basin oscillations between the sand ridge and the beach (Fig.01), the kind of reflection at both sides of the basin can be supposed to be positive, although the ridge is an underwater structure. This is because significant wave lengths are L > 40m >> 12m.

(Moreover it may be noted: Even in a *small scale* model basin, comprising of negative slope reflections (at phase shifts $90^0 < \Delta\varphi < 270^0$) at both sides, according to Fig.06 the same formula (1) is applicable as for Fig.03.)

Hence, the storm wave resonance at Sylt Island concerning the basin between beach and ridge (Fig.01), had reasonably been explained by the adapting lengths of neighboring frequency components to the existing boundaries, in using mode numbers basing on formula (1), although the distance dune – ridge at first sight cannot be related to the found wave lengths.

The anomalous behavior of the phase velocities corresponding with the above length adaptations, meaning that the ADE primarily consists in a *marked deviation from weak normal dispersion close to distinct resonance points*, had, however, not yet become sufficiently clear:

In [14] (and in further previous publications of this matter) the quasi measured *anomalous* dispersion function c(AD)(f) and the classical theoretic *normal* dispersion function c(ND)(f) had be contrasted with respect to the *total energy containing frequency range*. And the result had been considered to be sufficient for the proof of the resonance condition.

Possible doubts, on the one hand with regard to the measured phase velocities concerning the unsteady coherence function, or on the other hand with respect to the theoretical dispersion relation in view of doubtful estimated water depths, had been ignored.

By contrast first of all the *deviations* of the measured values of c(AD)(f) from the classical dispersion function close to the peak frequency f_P shall be put into the focal point of analysis and be illustrated exemplarily for measurement number 4 (dated December 13, 1973, 17:00) by Figures 07 to 12.

Actually the anomalous dispersion $dc/df > 0$ is strongest especially in the very narrow frequency band around the long-wave peak ($f_P \approx 0{,}09$Hz) combined with rather high coherence values. Moreover an ADE can also be recognized clearly for the second harmonic also together with high coherence at $f_{P2} \approx 0.18$Hz.

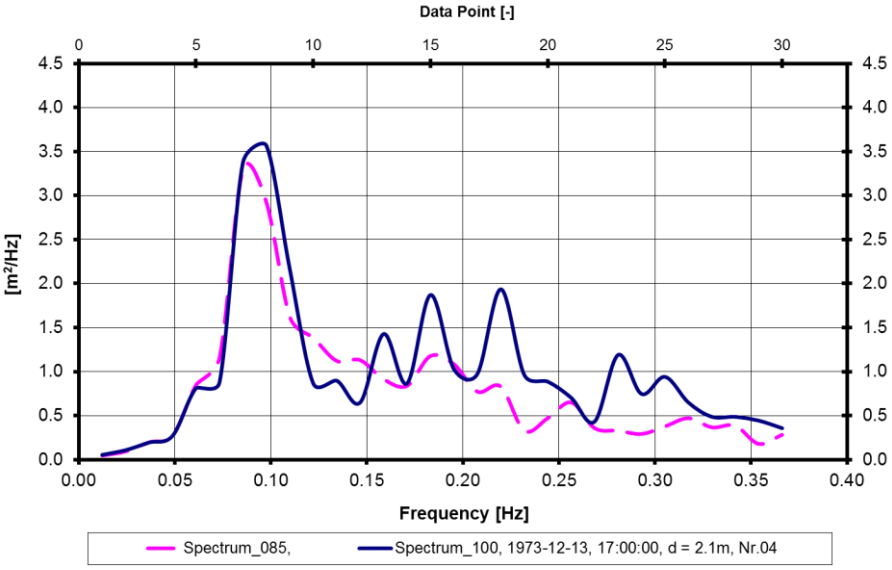

Fig.07: Synchronously measured energy spectra of storm waves at stations 100m and 85m. Measurement No. 4. Long wave peak at $f_p \approx 0.09$ Hz.

Similar to what is seen from Fig.05 regarding the wave tank investigations, also for the high energetic field measurements, it is *supposed* that the measured values of c(AD)(f) (respectively its best-fit curve) match the theoretical phase velocity c(ND)(f) in the very neighborhood of the resonance frequency $f = f_P$ according to the main peak.

Considering the conditions specified above, the water depth d in the classical dispersion function c(ND)(f) appears to be remarkably lower than that used for calculating the respective comparison function in [14] and [15] – namely $2{,}1 < 3{,}7$m. [2]

[2] The problematic nature concerning reliable *local water depths* is evidenced by comparing the image documents of appendices 4.1 and 4.2. Actually it can be seen that there was an immense removal of sand during the storm surges. Accordingly the water depths in [14] had been estimated *bigger* than they had actually been measured in [1] at station 100m in using a pressure sensor.
If, however, the phenomenon of anomalous dispersion is strictly seen in the above specified way as the *deviation from the theoretical normal dispersion function close to a resonance*

As to be seen from Figures 08 and 09, on the one hand the measured values of c(AD)(f) deviate from c(ND)(f) with increasing distance from the point of resonance with lower frequencies *downwards* and with increasing frequencies *upwards,* and on the other hand also the component lengths L(AD) close to the resonance frequency ($f_P \approx 0{,}09$Hz; first harmonic) tend to a *constant* value - though not so distinct as it is to be seen from Fig.05. Confidence in this case is documented by the impressive coherence value of $\bar{\gamma}^2_{xy}(f) > 0.9$.

For the purpose of further clarification in Figures 10 and 11 the line spectra of energy densities ED(L) are plotted with reference to stations 100m and 85m. Such values, related to discrete wave lengths had been calculated by summing up the single amounts of energy densities of frequency components having nearly equal wave lengths. With reference to station 100m the maximum energy density maxED(L) ≈ 10m²/Hz belongs to a wave length L(AD) = 47.6m (≈ 50m). By contrast in the frequency spectrum there is a maximum energy density of about maxEP(f) ≈ 3.6m²/Hz only, but the wave length (resonance wave length) is the same in both cases calculated for d = 2,1m (<3,7m) cf. Fig.10.

Fig. 11 contains additionally the phase velocity spectra of Fig.8 referring to wave lengths. In the spectrum $c_{(AD)}(L)$ the resonance is impressively marked by a jump according to $dc/dL \rightarrow \pm\infty$.

More detailed information can be found in reference no. [14] and [15]:

The 5 images of measurement No.4 contained in Annex 2a of [14] or in Figures 11 to 15 of [15] respectively, corresponding to Figures 7 through 11, meet approximately the resonance conditions of the *second harmonic* (at Coherence $\bar{\gamma}^2_{xy}(f) \approx 0.7$). Because in this case the point of intersection between c(AD) and c(ND) (belonging to water depth d = 3.7m > 2.1m) is very close to the resonance frequency f ≈ 0.18Hz respectively to the resonance wave length L ≈ 32.7m.

Note that quasi a bigger water depth is needed for the approximation of c(AD) and c(ND) close to the point of the second harmonic resonance than for the first harmonic resonance. This seems to be an indication that the classical dispersion relation is less adequate for 3-D high energy sea states than for the rather 2-D conditions in a wave tank.

By contrast, the *global anomalous behavior of the phase velocity* c(AD)(f), to be seen from Fig. 8, possibly can be explained by the fact that high energy spectra possess the peaks of *several* wave systems, whose points of resonance are close together, cf. Annex 4.4, Fig.09 and particularly measurements 9, 10 and 11 in reference No. [14].

By this reason perhaps also the similar phenomenon of global anomalous dispersion with reference to electromagnetic waves (spanning frequencies from radio waves to X-rays) can be explained, cf. reference [14], Fig.2 or [15], Fig.1 respectively.

frequency, the approximate water depth is found necessarily by the fact that the proper theoretical dispersion function can be calculated only by applying the *correct* water depth. If the later water depth (and phase velocity) is found in correspondence to the main peak, - according to the measurements - it matches the resonance points of the higher harmonics to a certain extent only.

In that sense, however, it cannot be started from the fact that the classical dispersion is valid in any case.

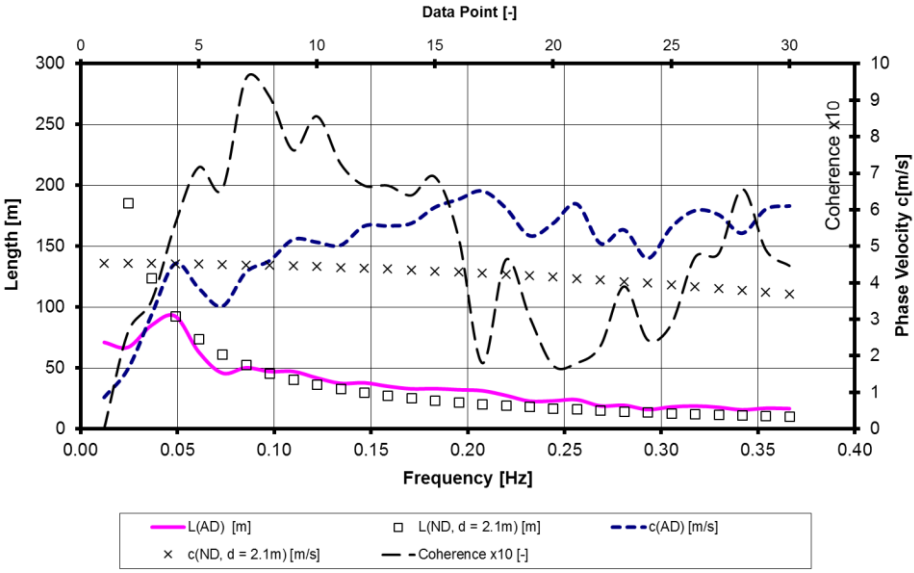

Fig. 8: Spectra of phase velocities c(f), lengths L(f) of frequency components and coherence $\bar{\gamma}^{2}_{xy}(f)$.,

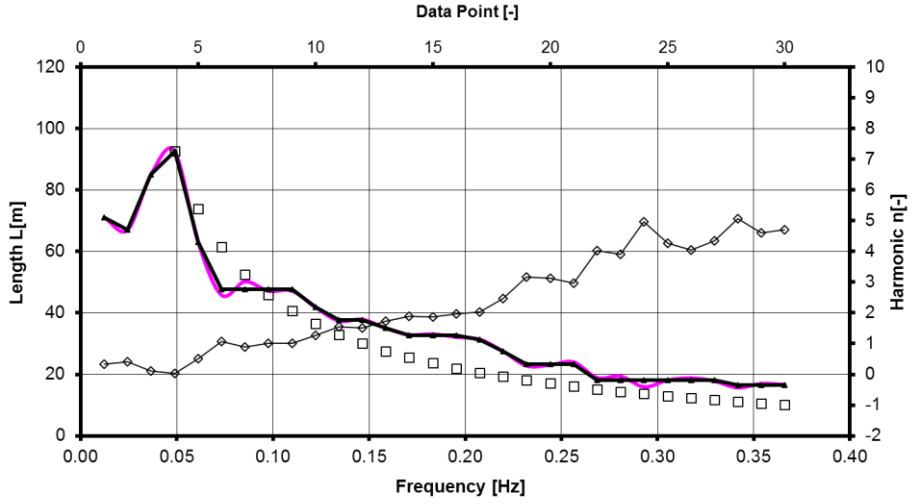

Fig.9: Magnified spectra of the lengths L(f) and of the order numbers n(f) of basin oscillations.

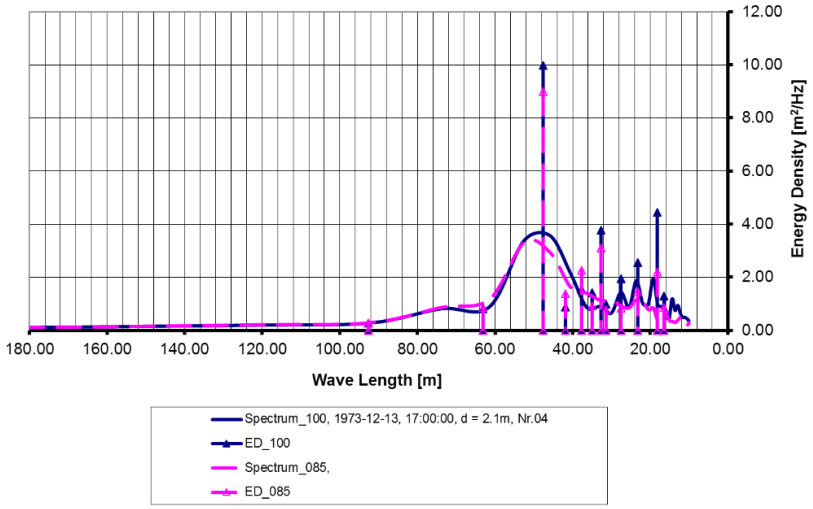

Fig.10: Energy Spectra transferred to the length axis in using the classical dispersion relation and Line Spectra of energy density ED(L) in using the Anomalous Length Spectrum L(AD)(f).

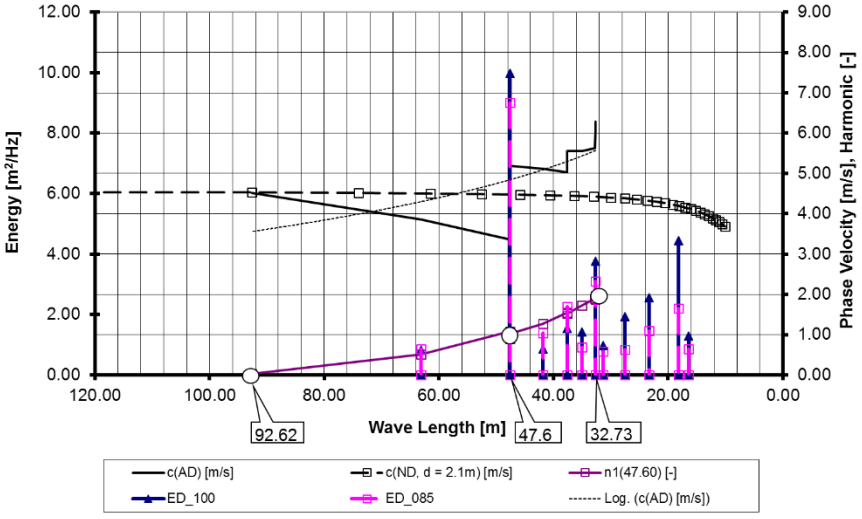

Fig.11: Phase Velocities c(ND)(L) and c(AD)(L), Harmonic Numbers n(L) and Line Spectra of Energy Density ED(L).

3. Formation of Partial Standing Waves

Contrary to the well-known harmful effects of wave reflection from Sylt's historical *nearly vertical* seawall, there are probably no papers on reflection effects from the dunes on the one hand and from the bluff between Wennigstedt and Kampen on the other.

In principle the *effect of wave reflection from natural coasts comprising of upstream-beaches* are still probably *underestimated* in relation to the other surf effects, because at such coasts reflection can achieve the upper hand only at a surge condition characterized by a *high water level* ***and*** a *steep slope formation*.

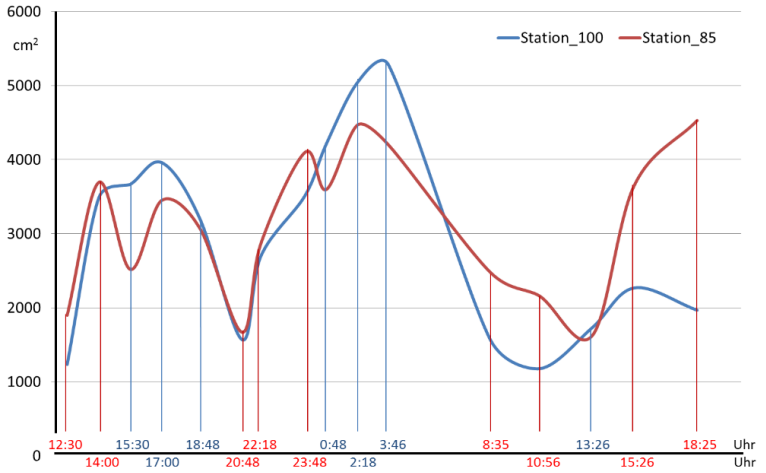

Fig.12: Spectral Energy $E = \sigma^2$ [cm²] of Frequency Range $0 \leq f \leq 3.125$Hz on December 13 and 14, 1973, comprising 16 measurement intervals, referring to measuring stations 100m and 85m [4]. Abscissa: Starting times of measurements.

In the following partial standing waves of considerable intensity - forming the essential preconditions of wave resonances – can be evidenced from the total evolution of the storm surge series.

For that purpose Fig.12 contains the cumulative spectrum energy $E = \sigma^2$ [cm²] (Integrated Spectrum Area) of the frequency range $0 \leq f \leq 3.125$Hz with reference to measuring stations 100m and 85m for the total measuring period of about 30 hours, cf. Appendix 4.3.

Similar graphical presentations of wave energy had yet been analyzed extensively in 1976 with respect to different frequency bands [4], [3].

(In order to emphasize the *rareness* of such high energetic storm surge recordings (with maximum energy densities of max E_{fP} = 4.38 m²/Hz and cumulated maximum energies of maxE = max $\sigma^2 \approx 5300$ cm²) in that publications also measurements had been documented representing attenuating cumulated wave energies of $E = \sigma^2 \approx 1100$ cm² at Beaufort 6 and $E = \sigma^2 \approx 650$ cm² at Beaufort 3).

At this place, once again the *temporary* phenomenon of a higher cumulative spectrum energy at station 85m (partly at breaking waves) than at station 100m (unbroken waves) shall be analyzed, cf. Fig.12. This time, however, especially considering *reflection effects* from the dune at high water levels.

Formerly this phenomenon had been explained solely by *refraction effects* due to waves focusing on station 85m.

Basing on the co-cumulative spectra (CCS) of the 16 measuring intervals with reference to the frequency range $0 \leq f \leq 3.125$Hz, there had not been sufficiently satisfactory statements except for the one that the energy of breaking waves is distributed over a wider frequency range.

By contrast basing on Figures 13 to 16, at this place criteria of differently unstable waves would be desirably derived from the degree of the gradient $dE/df > 0$.

While it is clear that increasingly higher frequencies are necessary for the representation of steepening and finally breaking waves, even higher frequencies will be needed for describing broken waves.

Figures 13 and 14 show the curves of different variances

$$E = \sigma_\eta^2 = \int_0^{f_i} G_{\eta\eta}(f)df$$

related to both measuring stations, representing the wave energies of i = 6 frequency ranges $0 \leq f \leq f_i$. The limiting frequencies are $f_1 = 0.05$Hz, $f_2 = 0.12$Hz, $f_3 = 0.2$Hz, $f_4 = 0.37$Hz, $f_5 = 1.0$Hz and $f_6 = 3.125$Hz.

In addition to the author's remarks in [3] and [4], at first a statement is given especially regarding the high frequency energy with respect to the wave stability.

Obviously phenomena of wave breaking are starting yet below 0.3Hz and produce energy densities up to rather more than 1Hz, cf. items 1-16 of Appendix 4.3. But surely wave induced energy densities will *not extend* to the maximum frequency $f_{max} = 3.125$Hz limiting the spectral calculations.

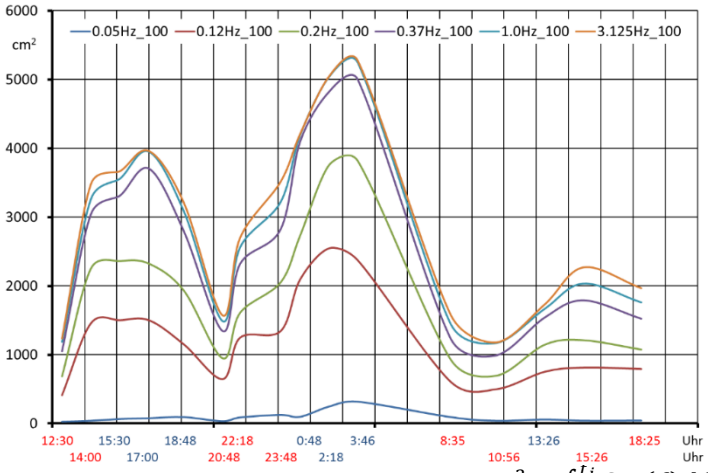

Fig.13: Distribution of the Measured Wave Energy $E = \sigma_\eta^2 = \int_0^{f_i} G_{\eta\eta}(f)df$ in i = 6 Partial Frequency Ranges on December 13/14, 1973 at station 100m.

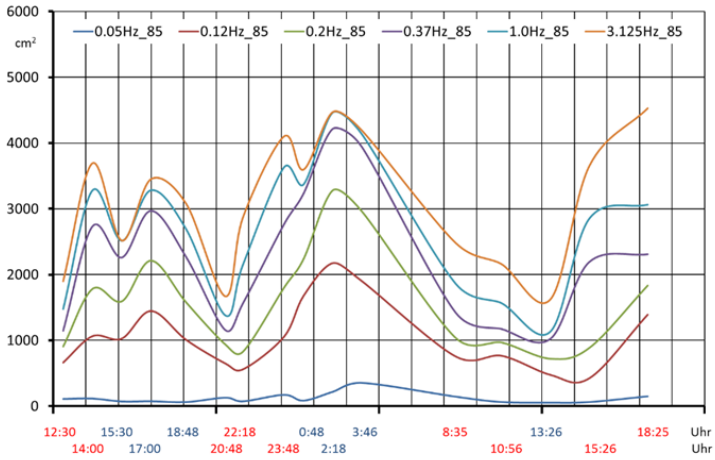

Fig.14: Distribution of the Measured Wave Energy E = $\sigma_\eta^2 = \int_0^{f_i} G_{\eta\eta}(f)df$ in i = 6 Partial Frequency Ranges on December 13/14, 1973 at station 85m.

Because the total analog raw data of the measurements, however, regrettably had been destroyed, the real upper limiting frequency 1Hz < f < f_{max} of wave induced energy densities can no longer be identified.

Moreover only speculation is possible on the *kind of wave breaking*, because statements on the position of partial standing waves relative to the effective point of reflection and respectively the phase of the complex reflection coefficient Γ (CRC) [18] , cannot be made.

The inspection of the energy in the high frequency partial range $1.0 \leq f \leq 3.125Hz$, however, is remarkable.

While big increases of energy in this range of maximum frequencies nearly occur all the time (at 14 of 16 measuring intervals, thus except at 15:30 and at 2:18) at station 85m (Fig.14), this is true to station 100m at low water levels only,- namely at intervals 14.00 – 15:30, 22:18 – 23:48 and 15:26 – 18:25.

Vice versa in this frequency range at highest water levels *only*, there is no significant increase of energy at station 85m, whereas this is the normal case at station 100m, except for the mentioned ones.

According to that factual circumstances, it can be concluded that energy shifts into this high frequency range at high water levels can be associated only with a partial wave instability, say *white capping*.

Intense wave breaking is, however, marked by high gradients dE/df in the partial frequency ranges neighboring downwards.

For instance in Fig. 15, it is demonstrated by measurement No 8 at station 85m that wave breaking is indicated by still increasing energy densities at frequencies above 0.3Hz and $dE\_85/df > 0$ even at f = 1.0Hz.

By contrast, there is almost no energy increase to be watched at station 100m at f = 1.0Hz. This is also true to the following measurements No 9 starting at 00:48, at both measuring stations, cf. Fig.16.

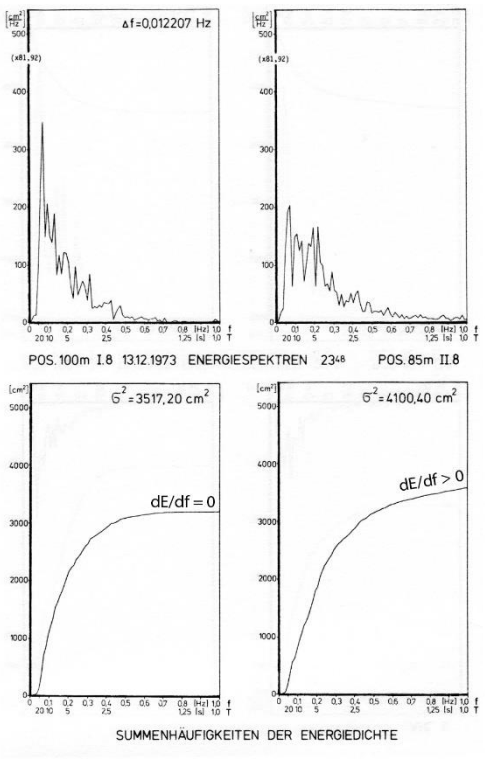

Fig.15: Energy spectra and Co-cumulative spectra of frequency range $0 \leq f \leq 1.0$Hz (Measurement No 8, Dec.13, 23:48). Energy of *breaking* partial standing waves at station 85m bigger than at station 100m.

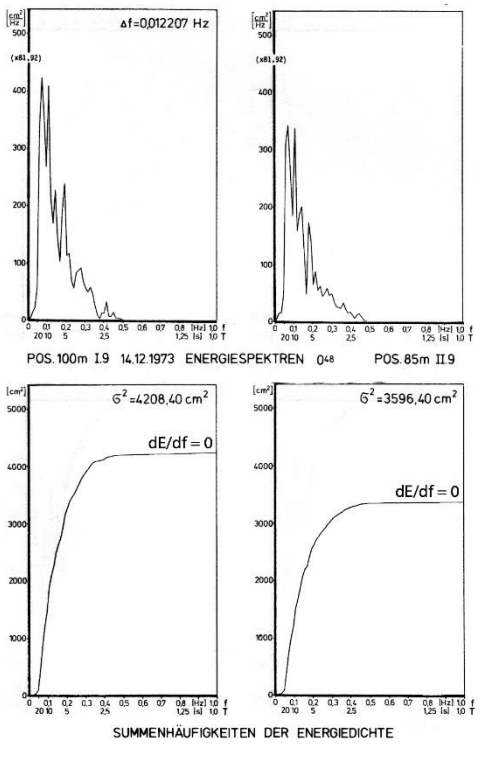

Fig.16: Energy spectra and Co-cumulative spectra of frequency range $0 \leq f \leq 1.0$Hz (Measurement No 9, Dec.14, 00:48). Energy of *non-breaking* partial standing waves at station 100m bigger than at station 85m.

Sea states characterized by the typical data configuration of Fig. 15, describing stable waves at station100m while there are breaking waves at station 85m, are of particular importance, because the co-cumulative spectrum belonging to station 85m shows a *bigger* energy content at f = 1Hz than that belonging to station 100m. Actually this condition is repeated by 9 of 16 measurements, cf. Appendix 4.3.

This is an indication that possibly the energy of the quasi stable waves of Fig.16 does not necessarily decrease from station 100m to station 85m merely due to friction effects, but energy containing partial standing waves are positioned such that their loops are close to station 100m or their nodes are close to station 85m respectively. Such conditions also apply to the remaining 7 measurements.

Vice versa, according to Fig.15 it is also plausible that there are small stable water level deflections close to a node of partial standing waves near station 100m, while the bigger water level deflections close to the loop of partial standing waves near station 85m combined with the smaller water depth at this location are responsible for breaking waves.

For demonstration purposes of the above reflection events, in the following once again reference is made to those measurements which had previously been analyzed with respect to the storm wave resonance [14]. They comprise 3 measurements each starting on December 13, 1973 at 15:30 and on December 14, 1973 at 0:48, assigned by maximum water levels exclusively.

That measurements are characterized by stable[3], non-breaking waves at both measuring stations, so that the energy decrease from station 100m to station 85m can largely be attributed to the phase difference of the partial standing waves existing with respect to the two stations.

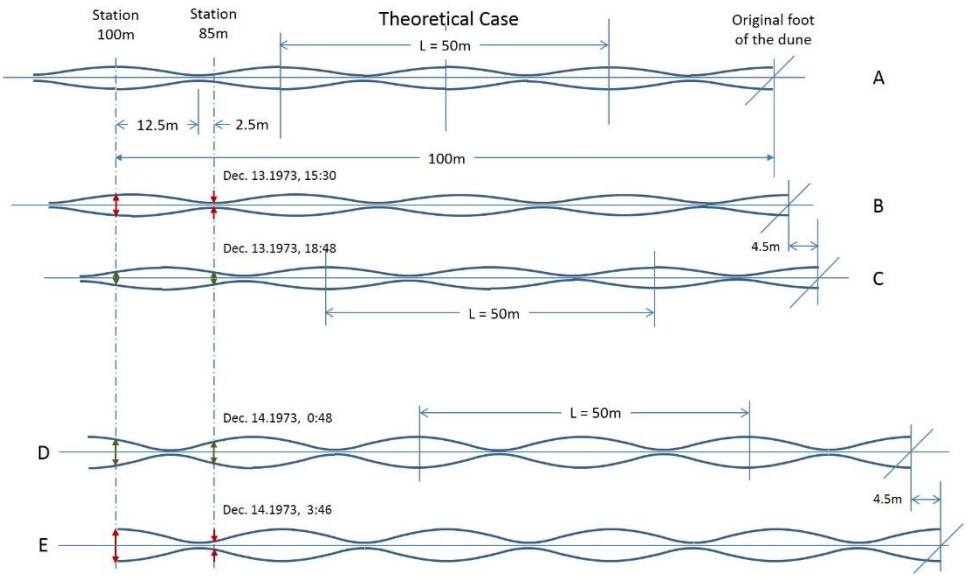

Fig.17: A. Theoretic start configuration: Partial standing wave of wave length L = 50m at the foot of the dune.
B. Red arrows: large water level deflections (wld) at station 100m, small wld at station 85m.
C. Green arrows: small differences of small wld at stations 100m and 85m.
D. Green arrows: small differences of big wld at stations 100m and 85m.
E. Red arrows: large wld at station 100m, small wld at station 85m.

For the measurements mentioned above the analyses in [14] had delivered resonant wave lengths in between 40 and 60m. (40m ≤ L ≤60m.) That is why exemplarily a wave length of 50m is used for the design of Fig.17. Moreover the wave length of measurement No 4 dated December 13, 1973, 17:00, interpreted by Figures 7 to 11, is rather close to this value.

Because of the fact that 3 storm surge events had happened in November and December 1973 just before the measurements, referred to here, had been carried out, a strong reference to the former origin of the coordinate system at the foot of the dune, cf. Fig.01, cannot be

[3] Water level deflections according to steep and broken Clapotis waves should be rare at the dune as well as at the ridge, because the slope angles sufficiently deviate from the vertical (in accordance with phase angle $\Delta\varphi \neq 0^{o}$ of positive reflection coefficient). Although breakers towards wave propagation direction can exist.

established. Actually the removal of material had caused a shifting of the foot of the dune by several meters landward, so that a detection of the former point of reflection was no longer possible.

In case, however, a partial standing wave of length L = 50m is assigned to the start configuration, according to case A in Fig.17, an incomplete loop could have rather been positioned close to station 100m and an incomplete node close to station 85m.

Except for the above claim of *positive reflection* at the dune (according to $90° < \Delta\varphi < +90°$) one can only speculate about a more precise position of the partial standing wave, because

- the exact position of the reflection point at the dune is unknown (origin of coordinates ≠ foot of the dune)
- the horizontal wave asymmetry and the upsetting deformation both increase with the approach to the reflection point, cf. [18] and [19]
- the position of the spectral peak is going to be changed due to superimposed accelerated currents.

In case, however, the *phase difference* referring to stations 100m and 85m is regarded as the *key determinant* with respect to this item, the *decreasing* difference $\Delta E \approx 1020 cm^2$ (= (3668,4 – 2518,2) – (3204,0 – 3074,4)) - within the time span 15:30 to 18:45 on December 13, 1973 - possibly can point to a coastward Clapotis shift of about 4 to 5m, cf. relative Clapotis positions B and C.

A similar result applies to the increasing difference $\Delta E \approx 468 cm^2$ (= (5277,6 – 4197,6) – (4208,4 – 3596,4)) - within the time span 00:48 to 03:46 on December 14, 1973.

Also a Clapotis shift of 4 to 5m is found, cf. relative Clapotis positions D and E.

Clapotis shifts of the magnitude mentioned above within a time span of about 3 hours (i.e. approx.1.5m/h) might be realistic to occur due to dune erosion during heavy storm surge conditions; especially at high tide levels accompanied by values of energy $E = \sigma^2 \geq 4000\ cm^2$, cf. Fig.02, and hence match a scenario characterized by reflection and resonance.

Finally it is intended to discuss once again the *variable distribution of the energy densities* within the *energy spectra* of the two measuring stations. This is also done for stable, non-breaking waves at both measuring stations only, so that the differences of energy densities at stations 100m and 85m should largely be attributed to the *differing phase differences* of the partial standing waves existing with respect to the two stations and are not caused by surf effects.

The treatment of the water volume, covering the beach and the foreshore area, as a basin's oscillating content, is important, because its maximum amplitudes (displacements) can only occur at places corresponding to the loops of partial standing waves. Hence it is clear that probably *not the maximum* energies are included in the present analysis of measurements.

Contrary to the measurements 3, 4, and 5 at very high storm tide water levels on December 13, 1973, each characterized by *one dominant peak* in the frequency range $0{,}073 \leq f_1 \leq 0{,}11 Hz$ (see Fig.7-11), on December 14, 1973 at even higher water levels at least *2 dominant wave systems* can be identified from the sequence of the measurements 9, 10 and 11 (see Appendix 4.3) each possessing different higher harmonics.

From the measurements 9 (starting 0:48) and 11 (starting 3:46), characterized in [14] by *bimodal energy spectra*, spots of resonance had been derived by the shape of the functions c(AD)(f) corresponding to harmonics numbers 0 to 3 for each of the two wave systems.

In Figures 18 to 20 of the present publication, this feature is examined further with respect to measurement no. 10, characterizing the *broad unimodal energy spectrum* with the maximum energy densities measured at all.

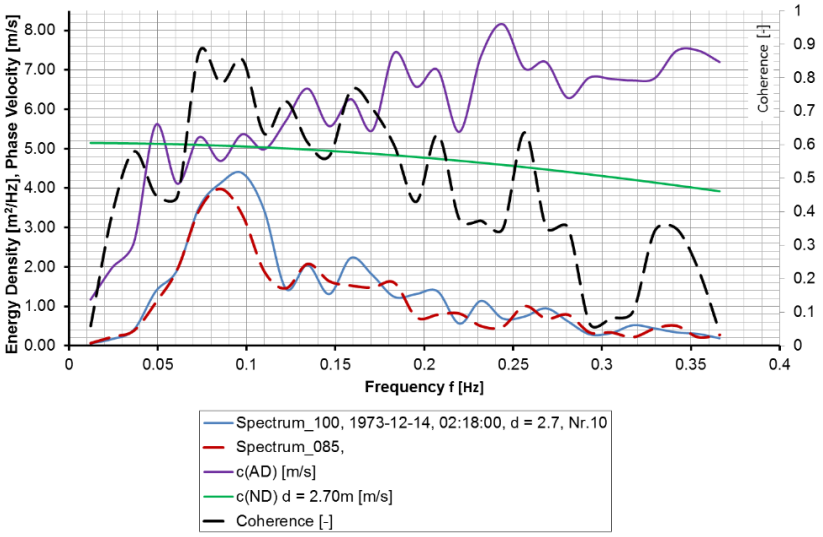

Fig. 18: Energy Spectra of measurement No. 10. Quasi measured oscillatory phase velocity function c(AD) at considerable Coherence values, to be compared with c(ND) according to the classical dispersion relation.

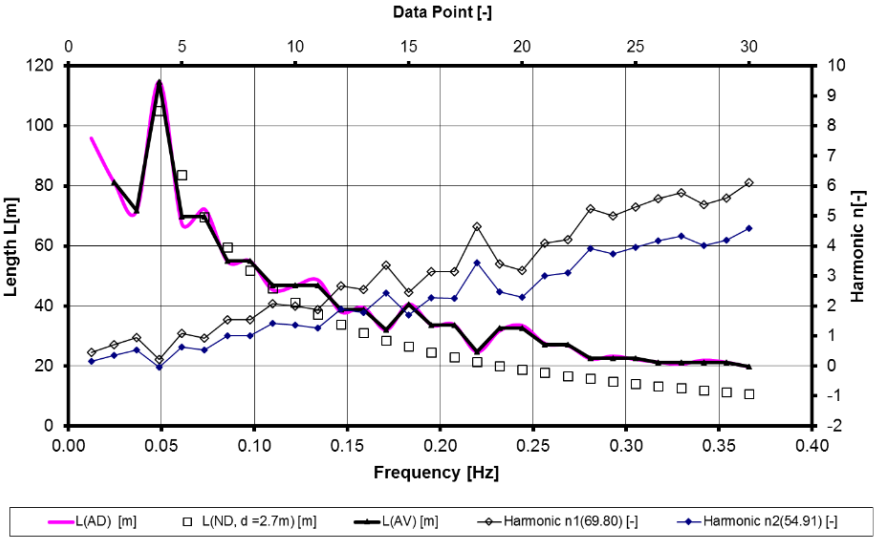

Fig. 19: Component length spectra L(f) together with ordinal harmonic numbers n(f). L(AV)(f) denotes the smoothed values of L(AD)(f) and L(ND)(f) are the theoretical values according to water depth d = 2.7m. The harmonic ordinal numbers of basin oscillations are characterized by the lengths of the first harmonics given in the figure.

In Fig.18 the energy spectra of measurement No. 10 are shown together with the quasi measured (*oscillatory) phase velocity* function c(AD)(f) and the Coherence-function. Additionally c(ND)(f) is plotted according to the classical dispersion relation

The wave length spectrum L(AD)(f) derived from c(AD)(f) is to be seen in Fig.19 together with a smoothed (linearized) version L(AV)(f) to be compared with the *theoretical* length spectrum L(ND)(f) calculated for water depth d = 2.7m.

Moreover the harmonic ordinal numbers of the two wave systems according to formula (1) basing on the first harmonics ($L_{1A} \approx 69.8$m and $L_{1B} \approx 54.91$m respectively) are shown. The second harmonics wave length are $L_{2A} \approx 46.89$m and $L_{2B} \approx 38.73$m.

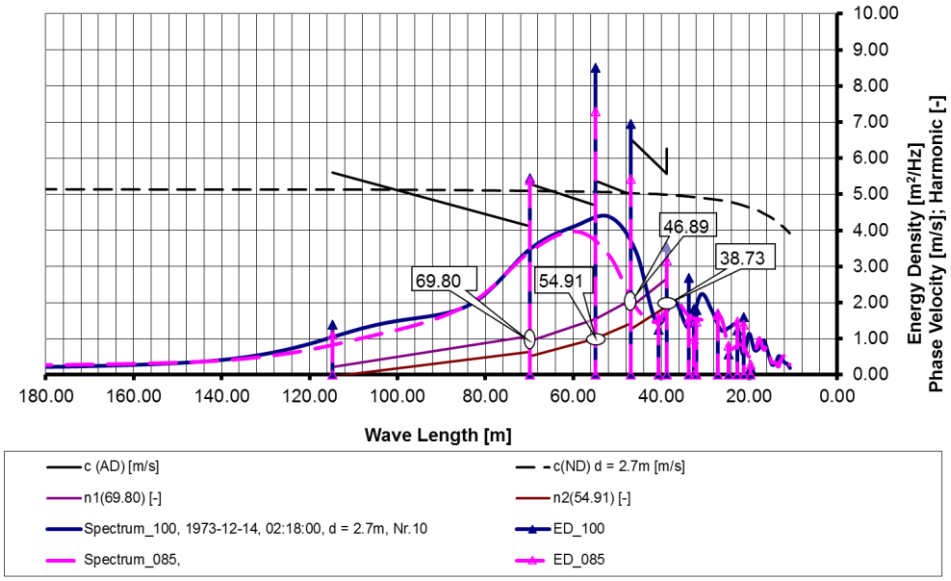

Fig.20: Energy density spectra transformed to the length axis in using the classical dispersion relationship. Line spectra of the energy density ED(L), calculated on the basis of the anomalous Length Spectrum L(AD)(f). Also the phase velocities and the ordinal numbers of the harmonic basin oscillations are plotted with reference to the wave lengths.

Hence, the broad peak can be attributed notably to the presence of 4 resonance points belonging to the first and second harmonics of the two wave systems. This could yet have been read from the 4 oscillations in the phase velocity plot c(AD)(f) of Fig.18 in the frequency range $0{,}05 \leq f \leq 0{,}135$Hz.

Using the generation law L(n) = L(n=0)/(n+1) the lengths of the fundamentals can be estimated as $L_{0A} \approx 140$m and $L_{0B} \approx 115$m. With respect to the distance beach – ridge, such values apparently are of some relevance, because energy density is still remarkable at those frequencies.

Fig.20 shows the transformation of the data from Figures 18 and 19 to the lengths – axis. Such a presentation seems to be useful, because the resonance points are marked not only by

the ordinal numbers of the harmonics but also by jumps in the function of the phase velocities c(AD)(L).

It is particularly noteworthy that not only multimodal but also (wideband) unimodal energy density spectra can be formed by *several neighboring points of resonance* especially at high energetic storm surges. Such conditions can be identified by the feature that alternating sections of anomalous and normal dispersion exist in the frequency range of considerable energy densities.

Because of such a feature also the global (*averaged)* anomalous dispersion considering nearly the whole energy containing frequency range, can be explained, which is similar to adopting smoothing techniques on the total electromagnetic spectrum in between radio waves and X-rays, cf. Abb.2 in [14] or Fig.1 in [15].

A separate treatment on resonance and anomalous dispersion is contained in [23]

4.1 A p p e n d i x 1: Image Documents of the wave measurement profile before storm surges of December 13, 1973

Condition of the measurement profile after 3 storm surge periods in November 1973, 19/20 and 24/25 and in December 1973, 6/7.

Sand-material, eroded from the foot of the dune, had deposited on the beach massively. Because measuring devices and cables covered by sand had to be exposed by engine power, some sand depots had been created, see Image 1.

Since most of the measuring devices had given up just during the preceded storm surges, at station 85m a two channel electromagnetic current-meter and wave gauges at stations 85m and 100m only had been available for data recording on electromagnetic tape on December 13/14.

Image 1: Seaward measuring stations at 60m, 80m and 100m.
Stations 120m and 128m damaged.

Image 2: Guide of the cable route on the seaward dune slope and underfloor the beach along the piles of the measuring stations 0m, 20m and 40m.

Image 3: Boardwalk positioned little landward from the foot of the dune close to the reference-zero-point of the measuring profile, which is marked by pile station 0m. Guide of cables below the boardwalk planking.

Photographs taken on Dec. 11, 1973

4.2 A p p e n d i x 2: Image documents of the wave measurement profile *after* the storm surges of December 13/14, 1973.

Image 4: The high pile marks the measuring station 40m at low water level.

Image 5: Relative locations of the boardwalk and the eroded foot of the dune.

Image 6: Eroded dune section landward of the boardwalk.

During the storm surge period enormous quantities of sand had been eroded from the beach and had been flushed into the sea, with the consequences that the cables had been excavated and sag freely between supports of distance 5m, see Image 4.
Because of the loss of sand from the beach, at mean high water level the wetting of the beach extends to measuring station 20m (see the snow-covered area at the right side of Image 4).

Erosion by waves locally had produced much steeper slopes at the foot of the dune, which was the reason, why the cables had to be untangled and re-positioned on the beach (Image 6) instead of their previous location very close to the planking of the boardwalk, see Image 3.

The supporting structure of the boardwalk is exposed to the open air nearly on the total former foundation depth (about 3m), with the consequence that its stability is no longer preserved and the structure had failed yet partly.

The relocation of the dune´s foot due to erosion during the storm surges is estimated to approx. 12m.

Approx. time of photographs taken: Dec. 15, 1973.

4.3 Appendix 3: Spectral FunctIons

Energy spectra and co-cumulative spectra of frequency ranges $0 \leq f \leq 1$Hz [4] belonging to measuring stations 100m and 85m. Each of the 16 data sets also includes the numerical values of the variances σ^2 with reference to the maximum calculation frequency 3.125Hz.

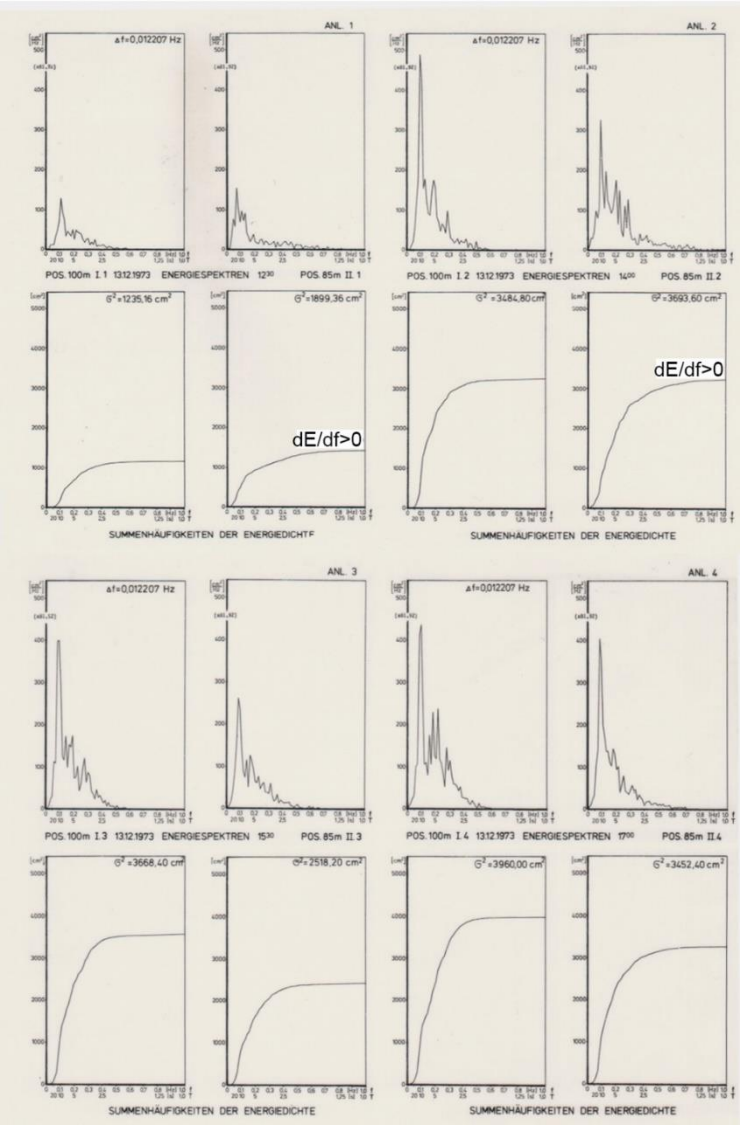

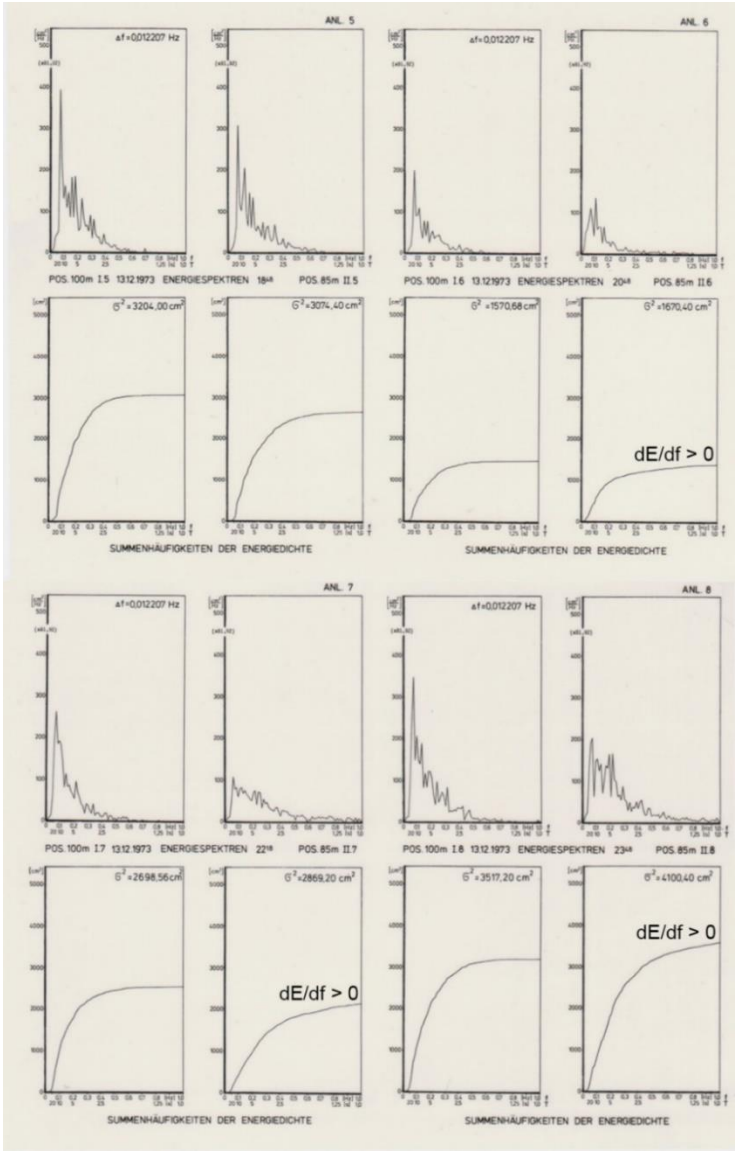

Real measuring units of energy density [m^2/Hz] requiring the ordinate value multiplied by 0.008192.

At measuring stations 85m, the marked gradients dE/df > 0 refer to 1Hz and indicate more or less intensely breaking waves.

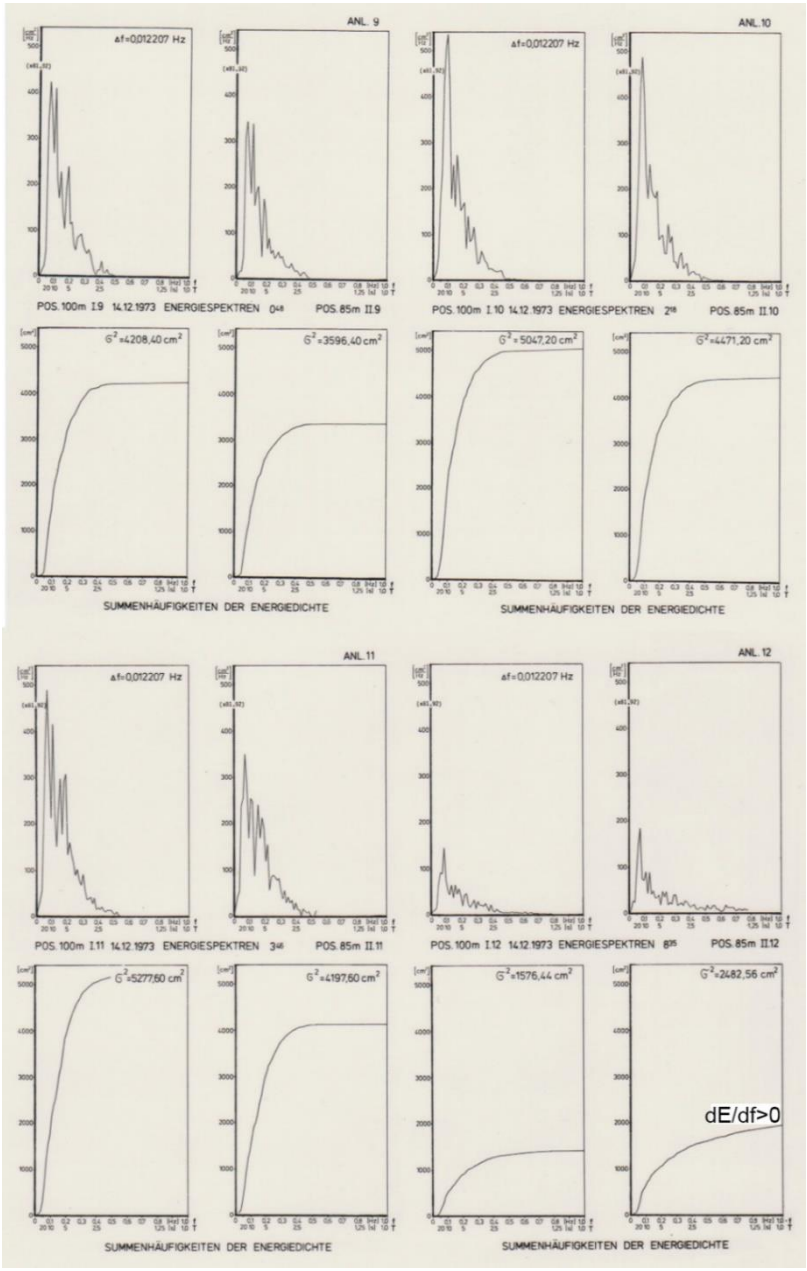

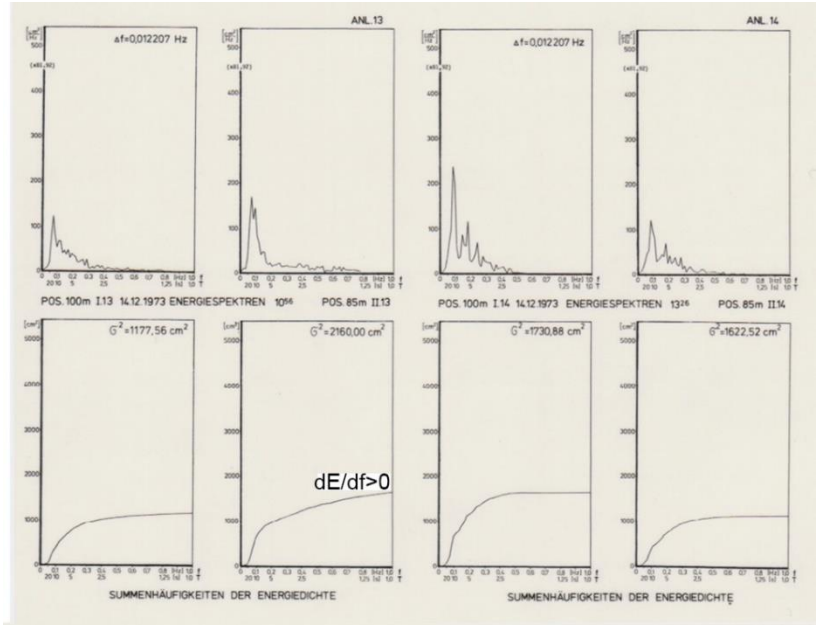

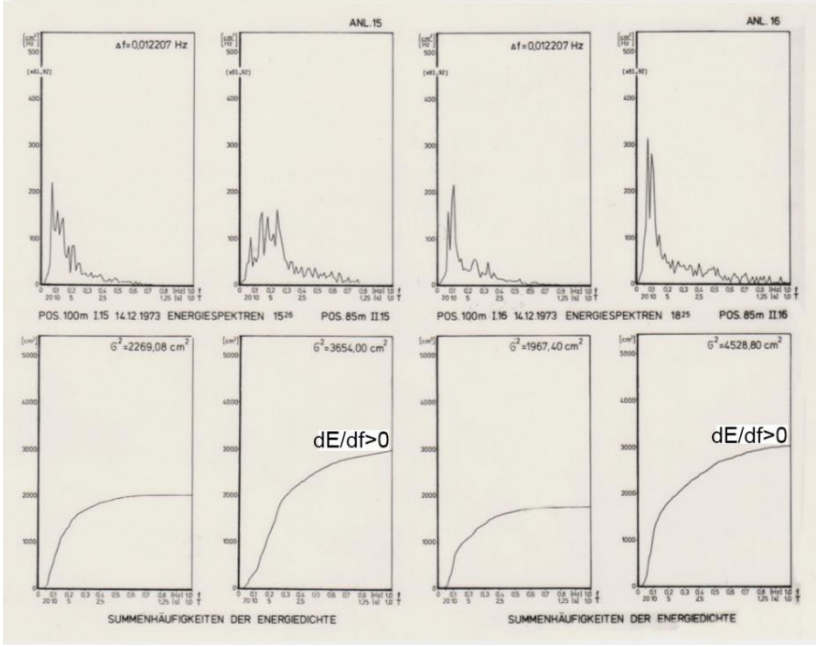

4.4 A p p e n d i x 4: Image documents of wave measurements in the winter season 1973 at the western coast of Sylt Island.

Image 7: Measuring profile at the beginning of the measuring campaign: Breaking and broken waves at Mean High Water (MHW).

Image 8: Plunging breaker at MHW positionend seaward of pile 100m

During the storm surge period Dec. 13/14,1973 exclusivly coastward of pile 100m.

Image 9: Plunging breaker produced by two wave systems.

5. Literature

[1] F. Büsching, „Über Orbitalgeschwindigkeiten irregulärer Brandungswellen," *Mitteilungen des Leichtweiß-Instituts für Wasserbau der TU Braunschweig, H. 42,* pp. 0-256; http://www.digibib.tu-bs.de/?docid=00057951, 1974.

[2] A. Führböter und F. Büsching, „Wave Measuring Instrumentation for Field Investigations on Breakers," *Proc. Ocean Wave Measurement and Analysis, Vol. I, New Orleans, USA,* pp. 649-668, http://www.digibib.tu-bs.de/?docid=00056512, 1974.

[3] F. Büsching, „On Energy Spectra of Irregular Surf Waves," *Proceedings, 15th Internat. Conference on Coastal Engineering, Honolulu, Hawaii, USA,* pp. 539-559; http://www.digibib.tu-bs.de/?docid=00056915, 1976.

[4] F. Büsching, „Über die Änderung von Wellenperioden im Brandungsbereich (Verteilung der Wellenenergie in Brandungsspektren)," *Mitt. des Leichtweiß-Instituts, H.47, TU Braunschweig,* pp. 122-164; http://www.digibib.tu-bs.de/?docid=00045452, 1975.

[5] F. Büsching, „Anomalous Dispersion of Surface Gravity Waves in the Near Shore Zone," *Proceedings 16th International Conference on Coastal Eng., Hamburg,* pp. 247-267; http://www.digibib.tu-bs.de/?docid=00056918, 1978a.

[6] F. Büsching, „Wave Deformation due to Decreasing Water Depth," *Mitt. des Leichtweiß-Instituts, H.63, TU Braunschweig,,* pp. 167-217; http://www.digibib.tu-bs.de/?docid=00045508, 1978b.

[7] F. Büsching, „Anomale Dispersion zur Darstellung der küstennahen Wellenverformung," *Die Küste,* Bd. 34, pp. 159-183; http://www.digibib.tu-bs.de/?docid=00047034, 1979.

[8] F. Büsching, „Doppler Aspects of Near-Shore Wave Transformation," *EUROMECH 114, Wladyslawowo, Poland,* pp. 1-6, 1980a.

[9] F. Büsching, „Neue Aspekte bei der Beurteilung küstennaher Wellentransformation und Energieumwandlung," *8. Aufbauseminar MEERESTECHNIK, TU Berlin,* pp. D1-D22; http://www.digibib.tu-bs.de/?docid=00049347, 1980b.

[10] F. Büsching, „Analogous Dispersion Properties of Surf Zone and Electromagnetic Waves," *Proceedings 18th International Conference on Coastal Eng., Capetown, South Africa,* pp. 154-171; http://www.digibib.tu-bs.de/?docid=00056917, 1982.

[11] F. Büsching, „Resonance Absorption Phenomena of Surf Zone Wave Kinematics," *1). Proceedings, 20th I.A.H.R.-Congress, Vol.VII, Moscow, USSR. 2). Proceedings, OCEAN ENGINEER-ING VII, Taipei, Republik China,* pp. 141-145, 12pages; http://www.digibib.tu-bs.de/?docid=00053995, 23-24 September 1983.

[12] F. Büsching und N. Speranski, „Dispersionseffekte bei Schwerewellen im Flachwasser," *Die Küste, H. 58,* pp. 161-177; http://www.digibib.tu-bs.de/?docid=00047795, 1996.

[13] N. Speranski und F. Büsching, „Dispersion Effects of Shallow Water Gravity Waves," *Bielefeld Univ. of Applied Sciences, Architektur & Bauingenieurwesen.*

Papers on Coastal Engineering, pp. 1-18; http://www.digibib.tu-bs.de/?docid=00047043, 1996.

[14] F. Büsching, „Sturmwellenresonanz an der Westküste der Insel Sylt," *Die Küste, H. 67,* pp. 51-82; http://www.digibib.tu-bs.de/?docid=00047046, 2003 .

[15] F. Büsching, „Wave Resonances Detected in a Wave Tank and in the Field.," *Fifth International Symposium WAVES 2005, Madrid, Spain,,* pp. Paper number 134. p. 1-12 & 1-2.; http://www.digibib.tu-bs.de/?docid=00043938, 3 - 7 July 2005.

[16] F. Büsching, „Phasensprung bei der partiellen Reflexion irregulärer Wasserwellen an steilen Uferböschungen," *HANSA, H.5 sowie Binnenschifffahrt, H. 9 & 10,* pp. 87-98 bzw. 73-77; http://www.digibib.tu-bs.de/?docid=00056885, 2010.

[17] F. Büsching, „Phase Jump due to Partial Reflection of Irregular Water Waves at Steep Slopes," *Proc. 3rd Int. Conf. on the Application of Physical Modelling to Port and Coastal Protection, COASTLAB 2010, Barcelona, Spain,* pp. Paper no. 67, pp 1 - 10; http://www.digibib.tu-bs.de/?docid=00047044, 28th - 1st September & October 2010.

[18] F. Büsching, „Komplexe Reflexionskoeffizienten für Wasserwellen - Zur Klassifiziereung von Brandungseffekten an Küstenschutzbauwerken -," *Die Küste, H. 78,* pp. 235-258; http://www.digibib.tu-bs.de/?docid=00047022, 2011.

[19] F. Büsching, „Complex Reflection Coefficients of Water Waves - On the Classification of Types of Breakers -," *Proc. Coastlab 12, 4th Int. Conf. of the Application of Physical Modelling to Port and Coastal Protection, Ghent, Belgium,* pp. 99-108, Extended Version 16 pages; http://www.digibib.tu-bs.de/?docid=00045344 ; ppt: http://www.digibib.tu-bs.de/?docid=00045521, 17-20 September 2012.

[20] W. Bascom, „Waves and Beaches," *Anchor Books; Doubleday & Company, Inc. Garden City, New York,* pp. 0-267, 1964.

[21] N. P. Holliday und et al., „Were extreme waves in the Rockall Trough the largest ever recorded?," *Geophysical Research Letters,* Nr. Vol. 33, L05613, p. 4 pages, 2006.

[22] J. Chappell und Wright, L. D., „Surf Zone Resonance and Coupled Morphology," *Proc. 16th Coastal Engineering Conference, Hamburg, Germany,* pp. 1359-1377, 1978.

[23] F. Büsching, „Resonanz und Anomale Dispersion bei Wasserwellen," *Digitale Bibliothek Braunschweig; Publikationsserver der TU Braunschweig,* pp. 1-14; http://www.digibib.tu-bs.de/?docid=00056747, 2014.

Image documents of Appendices 4.1, 4.2 and 4.4 had been taken from the author´s Kit Super Pro-videos.